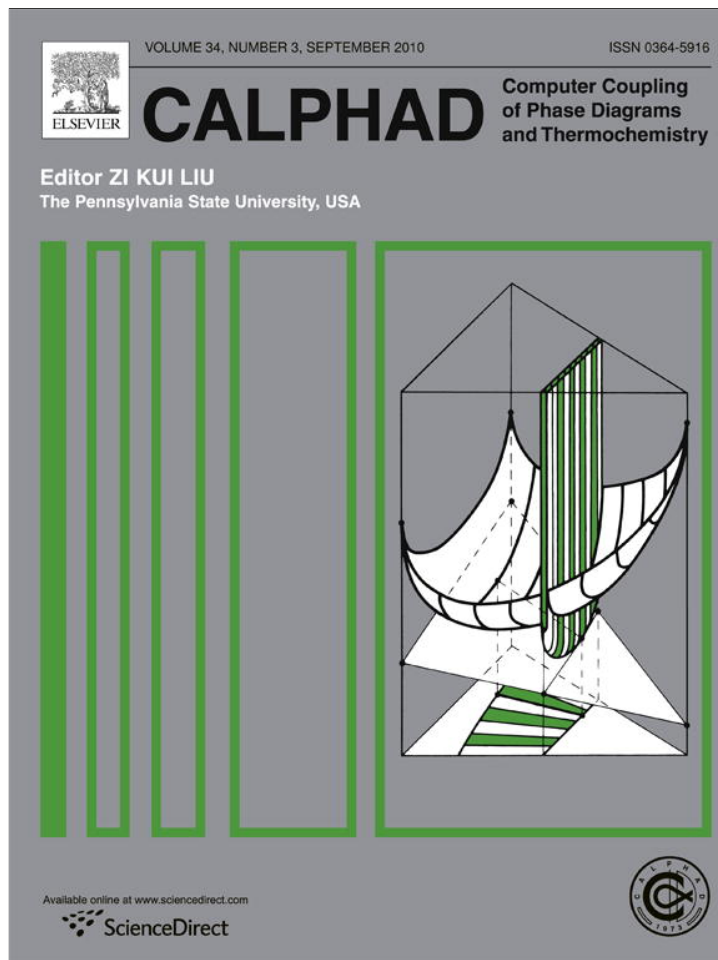


Provided for non-commercial research and education use.
Not for reproduction, distribution or commercial use.



This article appeared in a journal published by Elsevier. The attached copy is furnished to the author for internal non-commercial research and education use, including for instruction at the authors institution and sharing with colleagues.

Other uses, including reproduction and distribution, or selling or licensing copies, or posting to personal, institutional or third party websites are prohibited.

In most cases authors are permitted to post their version of the article (e.g. in Word or Tex form) to their personal website or institutional repository. Authors requiring further information regarding Elsevier's archiving and manuscript policies are encouraged to visit:

<http://www.elsevier.com/copyright>



Contents lists available at ScienceDirect

CALPHAD: Computer Coupling of Phase Diagrams and Thermochemistry

journal homepage: www.elsevier.com/locate/calphad

Thermodynamic modeling of the Pd–S system supported by first-principles calculations

Rongxiang Hu^{a,b}, Michael C. Gao^{a,c,*}, Ömer N. Doğan^a, Paul King^a, Michael Widom^d

^a National Energy Technology Laboratory, 1450 Queen Ave SW, Albany, OR 97321, USA

^b Oak Ridge Institute for Science and Education, MC-100-44, P.O. Box 117, Oak Ridge, TN 37831, USA

^c URS, P.O. Box 1959, Albany, OR 97321, USA

^d Carnegie Mellon University, Pittsburgh, PA 15213, USA

ARTICLE INFO

Article history:

Received 13 March 2010

Received in revised form

8 July 2010

Accepted 8 July 2010

Available online 2 August 2010

Keywords:

CALPHAD

Pd–S

Phase diagram

Sulfur poisoning

Hydrogen separation

ABSTRACT

Sulfur poisoning of PdCu membrane alloys has promoted new alloy development that requires quantitative understanding of the thermodynamics of the Pd–Cu–S system. This study attempts to develop a self-consistent thermodynamic description of the Pd-rich Pd–S binary system using the CALPHAD approach, based on available phase equilibrium information and thermochemistry data. The optimized phase diagram and enthalpies of formation agree well with the experimental values and first-principles calculations. The phase stability of this system is further investigated using first-principles calculations, confirming that the five intermetallic compounds reported are stable phases. The present density functional theory (DFT) calculations using various exchange–correlation functionals, pseudo-potentials and settings demonstrate that using the PBEsol functional reproduces the experimental enthalpies and phase stability of S, Pd and Pd–S compounds acceptably, and is able to reproduce the lattice parameters nearly perfectly.

© 2010 Elsevier Ltd. All rights reserved.

1. Introduction

Due to their high hydrogen selectivity and permeability, Pd and Pd alloys have been widely investigated as promising hydrogen separation membranes, which are used in water gas shift (WGS) and steam reforming reactions for efficient conversion of methane to hydrogen [1–3]. Separation membranes are also an essential part of the gasification-based coal-to-hydrogen production process where sulfur poisoning seriously affects the hydrogen permeability of Pd and Pd alloys [4,5]. The hydrogen flux decreases dramatically after exposure to the hydrogen-sulfide-containing gas [6]. As reported [6], the critical amount of H₂S in the H₂S feed that completely inhibited H₂S permeation was approximately 300 ppm for Pd–Cu alloys and 100 ppm for Pd surfaces, respectively. Gao et al. [3] summarized the research topics on the poisoning mechanism. The adsorbed sulfur atoms are bound to hinder the dissociation of H₂S molecules [7] and to reduce the mobility of the hydrogen atoms on the Pd surface [8]. At high sulfur coverage, the formation of Pd–S bonds induces large positive binding energy shifts in the core and valence levels of Pd, which has a strong impact on the surface properties of Pd membranes [9]. On the

other hand, since the lattice constant of palladium sulfide is much larger than that of pure Pd, the structural stress leads to crack formation in Pd or PdCu alloy membranes [10]. In order to develop multicomponent PdCu-based alloys of improved sulfur poisoning resistance, it is crucial to understand the thermodynamics of the Cu–Pd–S system. Although the partial Pd–S binary phase diagram has been studied experimentally [11,12], a quantitative thermodynamic description of the Pd–S system is not available in the literature. In this study, the CALPHAD (an acronym for the Calculation of Phase Diagram) method is used to calculate the Pd–S binary phase diagram based on available phase diagram information and formation enthalpy data. The phase stability of this system is further studied using first-principles density functional theory (DFT) calculations which confirm the crystal structures of five intermetallic compounds and provide formation enthalpy data of these compounds for CALPHAD optimization.

2. Experimental data

2.1. Phase equilibrium data

Weibke and Laar investigated the Pd–S phase diagram in 1935 [11] and identified the phases Pd₄S, PdS and PdS₂, and a high-temperature β-phase between PdS and Pd₄S. Later, the β-phase was identified as Pd₃S [13]. Pd₁₆S₇ was found to be a cubic body-centered structure with 46 atoms in the cubic cell [14–16]. The crystal structures of these palladium sulfides are listed in Table 1.

* Corresponding author at: National Energy Technology Laboratory, 1450 Queen Ave SW, Albany, OR 97321, USA. Tel.: +1 541 967 5869; fax: +1 541 967 5845.

E-mail address: michael.gao@netl.doe.gov (M.C. Gao).

Table 1
Palladium sulfide crystal structure data.

Phase	Composition, at.% S	Prototype	Pearson symbol	Space group	Reference
Pd ₄ S	20	Pd ₄ Se	tP10	$\bar{P}4_21c$	[11]
Pd ₃ S	25	Pd ₃ S	oC16	$Ama2$	[13]
Pd ₁₆ S ₇	30.4	Pd ₁₆ S ₇	cI46	$I\bar{4}3m$	[14–16]
PdS	50	PdS	tP16	$P4_2/m$	[11]
PdS ₂	66.7	PdSe ₂	oP12	$Pbca$	[17]

Table 2
Enthalpies of formation of palladium sulfides from experiments and present first-principles calculations (kJ/mol of atoms).

Compounds	$\Delta H_f^{298\text{ K}}$ [19,20] ^a	$\Delta H_f^{298\text{ K}}$ [12]	$\Delta H_f^{638-795\text{ K}}$ [21] ^b	$\Delta H_f^{298\text{ K}}$ from [21]	$\Delta H_f^0\text{ K}$ (first principles) ^c
Pd ₄ S	-19.84 ± 2.240 [19]	-24.328	-25.74	-12.7	-22.8
Pd ₃ S	-24.125 ± 2.625 [19]	-27.317			-25.4
Pd ₁₆ S ₇	-25.221 ± 1.574 [19]	-36.601			-29.5
PdS	-39.05 ± 5.50 [19]	-43.175	-68.55	-37.55	-40.3
PdS ₂	-26.067 ± 4.20 [20]		-69.24	-29.24	-30.8

^a Referred to Pd (solid) and S (solid).^b Referred to Pd (solid) and S (gas).^c The PBEsol gradient-corrected exchange–correlation functional [23] is used.

A partial phase diagram was drawn by Matkovic in 1976 [16]. Later, Taylor [12] reported an improved phase diagram over the range 0–50 at.% sulfur, which was based on more data points obtained using differential thermal analysis (DTA). Microprobe analysis was also used to confirm the composition of the phases. The liquidus and other phase transformation temperatures were determined with 25 samples. Each sample was heated and cooled many times to obtain a consistent pattern of thermal behavior, and a long annealing time was used to remove possible metastable phases from the samples. The main difference between the phase diagrams determined by Matkovic [16] and Taylor [12] lies in the Pd₁₆S₇–PdS region. Matkovic showed two invariant reactions, corresponding to 898 and 912 K. The invariant reaction at 898 K was not detected after longer annealing time [12]; therefore, it is not included in this study. The Pd–S phase diagram was updated by Okamoto [18] in 1992 based on the work from Weibke [11] and Taylor [12]. Since there is no experimental phase diagram information on the S-rich side, current optimization is only performed on the Pd-rich side up to 50 at.% S.

2.2. Thermochemical data

Using the high-temperature mixing calorimetry method, Zubkov et al. [19] measured the standard enthalpies of formation of four palladium sulfides, namely PdS, Pd₄S, Pd₃S and Pd₁₆S₇, at 298 K using solid Pd and solid S as the reference states. These values are shown in Table 2, compared with the calculated values from [12,19,20] and the present first-principles calculations. Taylor [12] calculated the matte sulfur pressure over 913–1498 K and 20–50 at.% sulfur by measuring the sample weight loss with time. Combined with the result from EMF (electrochemical force method) measurement on low sulfur mattes, the standard free energies of solid and liquid sulfides from Pd (solid) and S (gas) at high temperatures were obtained [12]. One reason for the big discrepancy in the formation enthalpy data among these results [12,19–21] is the use of different reference states for sulfur. The other is due to the change in heat contents of elements and compounds between different reference temperatures. Since both Taylor's and Niwa's data were measured at high temperatures and Niwa's data [21] were referred to gas-phase sulfur, the free energies from [12,21] are not used for the present optimization. The enthalpies of formation from [12] have been converted to standard formation enthalpy at 298 K. The enthalpies of formation from [21] are converted to standard formation enthalpies at 298 K using the method described in [22], and the results are listed in Table 2. For example, the enthalpy of formation of PdS at T₁ is determined as

$$\Delta H_{\text{PdS}}^{T_1} = \Delta H_{\text{PdS}}^{298\text{ K}} + \left(\int_{298}^{T_1} C_{\text{PdS}} dT - 0.5 \int_{298}^{T_1} C_{\text{Pd}} dT - 0.5 \int_{298}^{T_1} C_{\text{S}} dT \right) \quad (2.1)$$

where C_{PdS} , C_{Pd} and C_{S} are the heat capacities of PdS, Pd and S, respectively. The heat capacities of elements (Pd, S) and compounds (PdS, Pd₄S, PdS₂) used for the conversion are taken from [20]. On the other hand, the enthalpy formation data from [19,20] were measured at 298 K and agree very well with the present first-principles calculations, and thus they are reliable and given high weight during optimization.

3. Thermodynamic modeling

3.1. Pure elements

The Gibbs energies of pure S and Pd in their stable and metastable/unstable states are taken from the Scientific Group Thermodata Europe (SGTE) pure-element database [24], with the reference state being the enthalpies of the pure elements in their stable states at 298.15 K and 1 atm, referred to as the Standard Element Reference (SER). Pd has only one crystal structure in the solid state, face-centered cubic (fcc) [25]. The structure of S in the SER is face-centered orthorhombic (Pearson symbol oF128, space group $Fddd$) [25]. At temperatures higher than 393.65 K, a monoclinic structure becomes stable instead (Pearson symbol mP64, space group $P2_1/c$) [25]. The enthalpy change for this allotropic phase transition is found to be 0.4 kJ/mol from the SGTE database.

3.2. Liquid phase

The liquid phase is modeled with a substitutional solution model:

$$G_m^L = x_{\text{Pd}} {}^0G_{\text{Pd}}^L + x_{\text{S}} {}^0G_{\text{S}}^L + RT(x_{\text{Pd}} \ln x_{\text{Pd}} + x_{\text{S}} \ln x_{\text{S}}) + {}^{\text{ex}}G_m^L, \quad (3.1)$$

where x_{Pd} and x_{S} are the mole fractions of elements Pd and S; ${}^0G_{\text{Pd}}^L$ and ${}^0G_{\text{S}}^L$ are the Gibbs energies of Pd and S in the liquid state. The excess Gibbs energy ${}^{\text{ex}}G_m^L$ is described by the Redlich–Kister polynomial [26]:

$${}^{\text{ex}}G_m^L = x_{\text{Pd}}x_{\text{S}}[{}^0a_L + {}^0b_L^T] + ({}^1a_L + {}^1b_L^T)(x_{\text{Pd}} - x_{\text{S}}) + ({}^2a_L + {}^2b_L^T)(x_{\text{Pd}} - x_{\text{S}})^2 + \dots, \quad (3.2)$$

in which ${}^n a_L$ and ${}^n b_L$ are the interaction parameters for the liquid to be optimized.

3.3. Stoichiometric compounds

Based on experimental phase diagram information [11,12,25], Pd₄S, Pd₃S, Pd₁₆S₇ and PdS are modeled as stoichiometric compounds. According to SGTE, the Gibbs energy of a stoichiometric compound Pd_xS_y is modeled with a polynomial function [27]:

$$G^{\text{Pd}_x\text{S}_y} = \frac{x}{x+y} {}^0G_{\text{Pd}} + \frac{y}{x+y} {}^0G_{\text{S}} + a + bT + cT \ln(T) + dT^2 + eT^{-1} + fT^3. \quad (3.3)$$

The coefficients a, b, c, \dots are the parameters to be optimized for each compound phase.

3.4. Thermodynamic optimization

The model parameters in Eqs. (3.2) and (3.3) are optimized using the PARROT module of Thermo-CalcTM [28], by minimizing the weighted sum of differences between calculated and experimental values using nonlinear least-squares regression. The weight for each experimental data point is set according to the experimental accuracy. The optimization starts with liquid: using the zeroth-order interaction parameters was found sufficient. Then the PdS phase was optimized using three parameters due to its very wide phase field. Pd₄S, Pd₁₆S₇ and Pd₃S compounds were then optimized sequentially using constant enthalpy and entropy parameters. A final touch-up optimization was done by optimizing all parameters simultaneously.

4. First-principles energy calculations

The Pd–S binary was further studied using the first-principles package of VASP 5.2 (Vienna *ab initio* simulation package) [29,30] which solves for the electronic band structure using electronic density functional theory. Ultrasoft (US) pseudo-potentials [31] and projector augmented-wave (PAW) potentials [32] were used as supplied with VASP, using a variety of density functionals. The Brillouin zone integrations were performed using Monkhorst–Pack k -point meshes [33], and a smearing parameter of 0.2 eV was chosen for the Methfessel–Paxton [34] technique. The reciprocal-space (k -point) meshes were increased to achieve convergence to a precision of better than 1 meV/at. All structures were fully relaxed (both lattice parameters and atomic coordinates) until the energies converged to a precision of 1 meV/at. A “high” precision setting was used, and the plane-wave energy cut-off was held constant at 500 eV. The semi-core 4p electrons of Pd were explicitly treated as valence electrons. Other settings such as “medium” precision and energy cut-off at 280 and 350 eV were also used, and the results are presented in the Appendix; they demonstrate that both the energies and the lattice parameters of pure sulfur are well converged with the setting of “high” precision and an energy cut-off of 500 eV.

The total energies at 0 K of pure Pd, S, and their binary compounds were calculated. Pure Pd, six allotropic structures of pure sulfur [35], and five Pd–S compounds [25,35] were examined. To obtain the enthalpy of formation values ΔH_f , a composition-weighted average of the pure-element cohesive energies is subtracted from the cohesive energy of a given composition. The resulting energy is an “enthalpy” because its volume is relaxed at zero pressure. The phase stability at 0 K is evaluated by a convex hull plot (see Fig. 1). Vertices of the convex hull of a scatter plot of ΔH_f versus composition identify stable structures.

Choosing a suitable density functional for Pd–S is a challenge owing to the lack of dispersion force in conventional DFT methods [36,37]. While this could be a serious limitation for

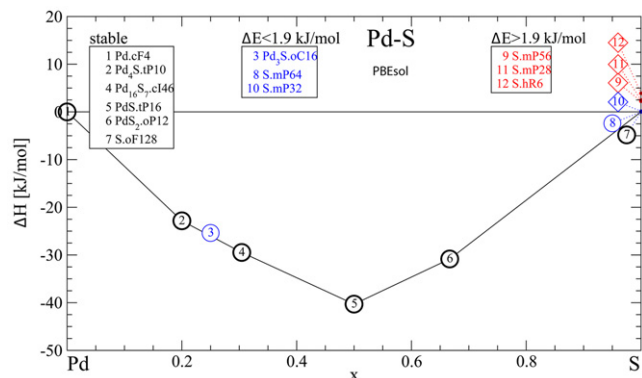


Fig. 1. (Color online) Convex hull plot of Pd–S alloys from the present DFT calculations using the PBEsol [23] gradient-corrected exchange–correlation functional. The plotting symbol notation is as follows: heavy circles for known stable, binary phases; light circles for known high-temperature phases; diamond for metastable structures. Tie-lines run along convex hull edges, joining low-enthalpy structures at the vertices of the convex hull.

elemental sulfur and sulfur-rich compounds, it is expected that the imperfection using these functionals should have less impact on the enthalpies of formation of compounds in the sulfur-poor sides (less than 50 at.% S) since the S–S atomic interactions are less important for those compounds. We tested several popular density functionals, namely the local density approximation (LDA) [38] using an ultrasoft (US) pseudo-potential [31] and PAW potentials [32], and the gradient-corrected exchange–correlation functionals of Perdew and Wang (PW91) [39], Perdew, Burke and Ernzerhof (PBE) [40], AM05 [41–43] and PBEsol [23]. The corresponding results are presented in the Appendix (in the following we adopt the notation [potential type]_[density functional] to specify the type of potential employed (e.g., US or PAW) and the density functional (e.g., LDA, PW91, etc.). The gradient-corrected exchange–correlation functional PBEsol [23] is used for the presentation in the main text since, as we show below, it is able to reproduce the experimentally observed phase stabilities and enthalpies well. Additionally, it reproduces the lattice parameters of pure sulfur and palladium sulfides nearly perfectly.

First, we tested the ability of different potentials and functionals to reproduce the experimentally known stabilities and lattice parameters of elemental sulfur. The low-temperature stable form of sulfur [35] is S.oF128 (The structure notation in this section is [prototype or chemical formula],[Pearson symbol], where the prototype is the name of some commonly known isostructural compound, and the Pearson symbol gives the point symmetry, translational symmetry and number of sites per unit cell). In addition, S.mP64 is the high-temperature stable form, and Pearson types mP28, mP32 and mP56 are presumably metastable forms. The present calculations using the PBEsol functional predict that the energies of S.mP64 and S.oF128 are nearly identical within computational uncertainty (see Fig. 1 and Table A.1), while S.mP32 has a slightly higher energy than them by 0.2 kJ/mol. Calculations using both PAW_PBE and PAW_PW91 potentials incorrectly predict that S.mP32 and S.mP64 both have lower energies than S.oF128 (Table A.1). On the other hand, the calculations using both US_LDA and PAW_LDA potentials correctly predict the sequence of phase stability of sulfur; that is, S.oF128 is stable at the ground state and S.mP64 has a higher energy by 0.4 kJ/mol. The S.hR6, S.mP28 and S.mP56 structures are all metastable structures and indeed they all are predicted to have much higher energies than S.oF128, S.mP64 or S.mP32. The calculated lattice parameters of sulfur using various DFT functional and settings are presented in Table A.2. Using US_LDA and PAW_LDA potentials underestimates the lattice parameters, while using PAW_PW91 and PAW_PBE

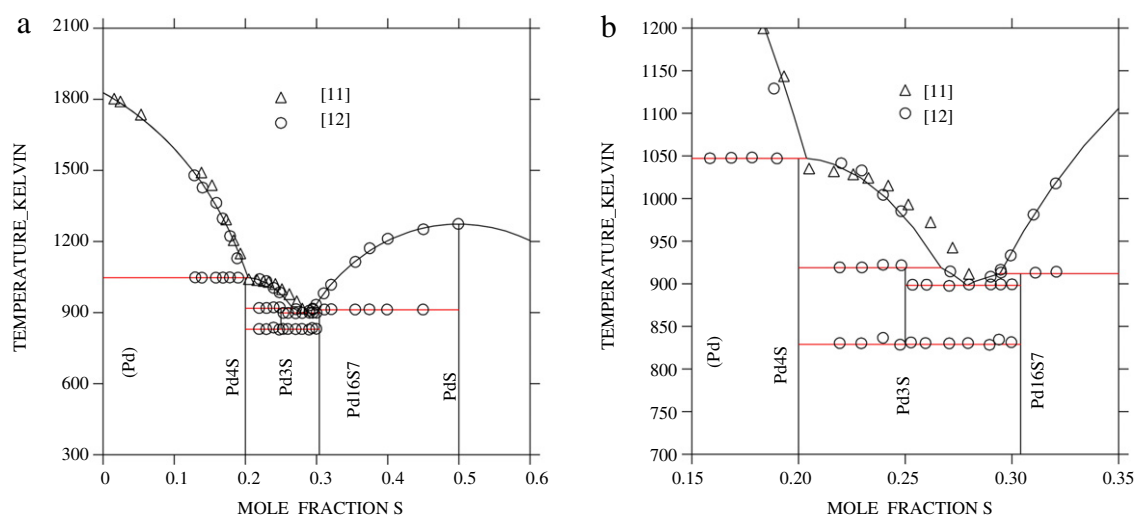


Fig. 2. (Color online) (a) Calculated Pd–S binary phase diagram from present CALPHAD modeling in comparison with available experimental data [11,12] over the composition range 0–55 at.% sulfur. (b) Enlarged portion over the range 15–35 at.% sulfur.

potentials overestimates the lattice parameters if compared to experimental data. Using the AM05 potential overestimates the lattice parameters the most. The calculated lattice parameters using the PBEsol functional agree excellently with experimental values, as intended by its design [23].

The calculated lattice parameters of palladium and palladium sulfides are presented in Table A.3 in comparison with experimental data. The calculated lattice parameter of Pd is largely insensitive to the choice of functional, pseudo-potential or the setting, although using PAW_PW91 and PAW_PBE potentials predicts that Pd is weakly ferromagnetic at the ground state with an atomic spin magnetic moment of ~ 0.3 Bohr magnetons. As expected, the calculated lattice parameters of all sulfur-poor palladium sulfides agree very well with experimental data regardless of the choice of functional, potential or the setting. As for PdS₂.oP12, excellent agreement is obtained only if the PBEsol functional is used. The resulting enthalpies of formation are displayed in Fig. 1 and the enthalpy values are listed in Table 2 and Table A.4. Pd₄S.t110, Pd₁₆S₇.cI46, PdS.tP16 and PdS₂.oP12 all lie on the convex hull and they are low-temperature stable phases in the experimental phase diagram. Pd₃S.oC16 lies slightly above it by 0.6 kJ/mol, and it is indeed a high-temperature phase. Similar results are obtained using US_LDA, PAW_LDA, and AM05 potentials (see Figs. A.1–A.3). However, using both PAW_PW91 and PAW_PBE incorrectly predicts that Pd₃S.oC16 lies on the convex hull (see Figs. A.4 and A.5).

The enthalpies of formation predicted by PBEsol agree with experimental values, yielding an RMS (root mean square) difference of calculation from experiment of 3.24 kJ/mol, similar to the experimental uncertainties. Additionally, PBEsol correctly predicts Pd₃S.oC16 as a high-temperature phase, in contrast to the PW91 and PBE GGA results. Finally, the lattice parameters of pure elemental sulfur in all its allotropes are correctly predicted only by PBEsol. Thus we selected the PBEsol functional as the basis for this study.

5. Optimization results and discussion

Fig. 2 shows the calculated Pd–S phase diagram over the range 0–50 at.% sulfur compared with available experimental data from the literature, including the liquidus and invariant reaction temperatures. As can be seen, the experimental phase boundaries are well reproduced by the present CALPHAD modeling. The liquidus over the range 20–30 at.% sulfur from Weibke et al. [11] differs slightly from that of Taylor [12]. The present modeling

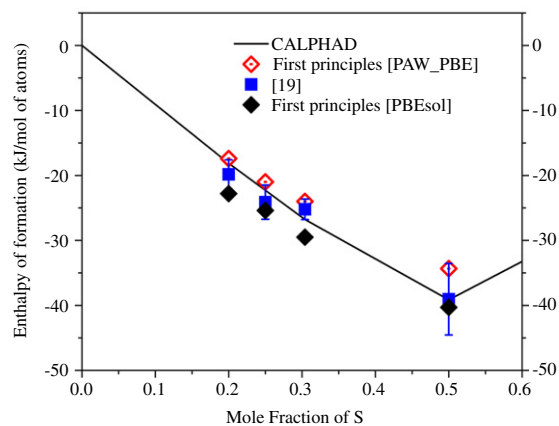


Fig. 3. (Color online) Calculated enthalpies of formation of binary palladium sulfides from the present CALPHAD modeling in comparison with available experimental data and the present DFT calculations using the PBEsol gradient-corrected exchange–correlation functional and PAW_PBE potentials.

Table 3
Optimized thermodynamic parameters for the Pd–S system.

Phase	Parameters	Optimized values (J/mol of atoms)
Pd ₄ S	$G^{\text{Pd}_4\text{S}} - 0.8^0 G_{\text{Pd}}^{\text{fcc}} - 0.2^0 G_{\text{S}}^{\text{ort}}$	$-18\,131 + 1.499T$
Pd ₃ S	$G^{\text{Pd}_3\text{S}} - 0.75^0 G_{\text{Pd}}^{\text{fcc}} - 0.25^0 G_{\text{S}}^{\text{ort}}$	$-21\,441 + 1.362T$
Pd ₁₆ S ₇	$G^{\text{Pd}_{16}\text{S}_7} - 0.696^0 G_{\text{Pd}}^{\text{fcc}} - 0.304^0 G_{\text{S}}^{\text{ort}}$	$-26\,780 + 3.295T$
PdS	$G^{\text{PdS}} - 0.5^0 G_{\text{Pd}}^{\text{fcc}} - 0.5^0 G_{\text{S}}^{\text{ort}}$	$-36\,086 - 69.478T + 10.227T \ln(T)$
Liquid	$^0 L_{\text{Pd,S}}^{\text{liquid}}$	$-152\,889 + 53.122T$

assigns higher weights to Taylor's data [12] since it is more accurate.

The calculated enthalpies of formation of palladium sulfides from this study are compared with the experimental data [19] and the present first-principles calculations using both PBEsol and PAW_PBE potentials, as shown in Fig. 3. All these data sets are in reasonably good agreement. The optimized thermodynamic parameters for the Pd–S system are summarized in Table 3. The invariant reaction temperatures and compositions calculated in this work are compared with the assessed values, as listed in Table 4. The difference in the invariant temperatures is all less than 1 K. The present study demonstrates that first-principles calculations can be used to assist CALPHAD optimization of phase diagrams in several ways [44–49]: (1) to assist verifying the crystal structures of all reported phases; (2) to provide reliable

Table 4
Invariant point comparison between assessed values [18] and the present calculation.

Reaction	Composition (at.% Sulfur)			Temperature (K)	Reference
L + (Pd) \leftrightarrow Pd ₄ S	20.5	0	20	1047	[18]
	20.37	~0	20.37	1047	This work
L + Pd ₄ S \leftrightarrow Pd ₃ S	26.5	20	25	919	[18]
	26.68	20	25	918.7	This work
L \leftrightarrow Pd ₃ S + Pd ₁₆ S ₇	28	25	30.4	898	[18]
	27.89	25	30.4	898.3	This work
Pd ₃ S \leftrightarrow Pd ₄ S + Pd ₁₆ S ₇	25	20	30.4	829	[18]
	25	20	30.4	828.9	This work
L + PdS \leftrightarrow Pd ₁₆ S ₇	29.5	50	30.4	912	[18]
	29.43	50	30.4	911.8	This work
L \leftrightarrow PdS	0	50	0	~1273	[18]
	0	50	0	1273	This work

Table A.1
Calculated total energies (kJ/mol) of sulfur with various exchange–correlation functionals with respect to S.oF128.

Ex. func.	ENCUT (eV)	Precision	S.hR6	S.mP28	S.mP32	S.mP56	S.mP64 ^a
US_LDA	500	H	1.8	1.6	0.7	1.3	0.4
US_LDA	247.2	H	1.7	1.6	0.6	1.3	0.4
US_LDA	197.8	M	1.2	1.4	0.6	1.1	0.3
PAW_LDA	500	H	1.7	1.6	0.7	1.3	0.4
PAW_LDA	350	H	1.6	1.5	0.6	1.2	0.4
PAW_LDA	280	M	1.5	1.4	0.6	1.1	0.3
PAW_PW91	500	H	6.1	4.0	−0.1	3.6	−0.2
PAW_PW91	350	H	6.1	3.9	−0.1	3.5	−0.2
PAW_PW91	280	M	5.9	3.2	−0.1	3.0	−0.4
PAW_PBE	500	H	6.2	3.7	−0.1	3.6	−0.2
PAW_PBE	350	H	6.2	3.7	−0.1	3.6	−0.2
PAW_PBE	280	M	6.1	3.4	−0.3	3.1	−0.5
PAW_PBE ^b	503	H	6.1	3.5	−0.2	3.4	−0.4
PAW_PBE ^b	402.4	M	5.9	3.8	−0.1	3.5	−0.1
PBEsol	500	H	4.0	2.5	0.2	2.2	0.0
PBEsol	350	H	4.0	2.5	0.2	2.2	0.0
PBEsol	280	M	3.9	2.3	0.1	2.0	0.0
AM05	500	H	6.7	3.8	−0.5	4.1	−0.1

^a The enthalpy change associated with the phase transition between S.oF128 and S.mP64 is found to be 0.4 kJ/mol from the SGTE database [24].

^b The hard sulfur pseudo-potential (S_h) is used. The standard sulfur pseudo-potential is used for all other calculations. “Ex. func.” signifies the exchange–correlation functional and potential.

formation enthalpy data for stable and hypothetical structures which can then be directly plugged into the CALPHAD database; (3) to expedite optimization since the enthalpy parameters do not need to be optimized; (5) to make database development more physically meaningful.

6. Conclusions

The Pd–S phase diagram in the composition range 0–50 at.% sulfur is modeled using the CALPHAD method. The calculated phase diagram and formation enthalpy data agree well with available experimental data. The present first-principles calculations confirm the crystal structures of five stable intermetallic compounds. The formation enthalpy data predicted from first principles agree well with experimental values, suggesting that first-principles calculations can be used to expedite CALPHAD optimization by providing reliable thermochemistry data for stable and hypothetical phases. The present DFT calculations using various exchange–correlation functionals, pseudo-potentials and settings demonstrate that using the PBEsol functional reproduces the experimental enthalpies and phase stability of S, Pd and Pd–S compounds acceptably, and it is able to reproduce the lattice parameters nearly perfectly.

Acknowledgements

This research was performed with the support of the Syngas and Hydrogen Program of the NETL's Strategic Center for Coal. This research was supported in part by an appointment (of R.H.) to the US Department of Energy (DOE) Postgraduate Research Program

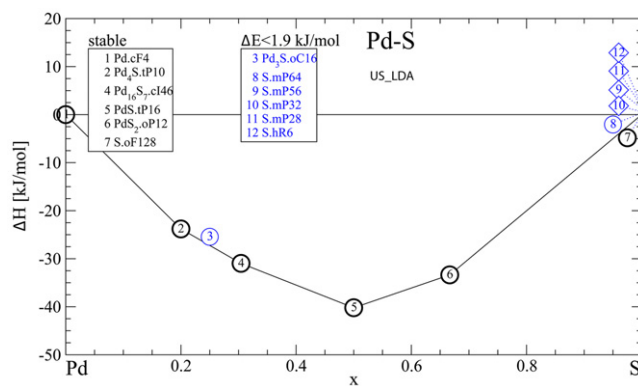


Fig. A.1. Convex hull plot of Pd–S alloys from the present DFT calculations using the US_LDA gradient-corrected exchange functional.

at the NETL administrated by the Oak Ridge Institute for Science and Education. Computational time was partially supported by Pittsburgh Supercomputing Center with Grant No. DMR080005.

Appendix A

See Tables A.1–A.4.

Appendix B. Supplementary data

Supplementary material related to this article can be found online at doi:10.1016/j.calphad.2010.07.002.

Table A.2
Calculated lattice parameters (Å and degrees) of elemental sulfur compared with experimental data.

Ex. func.	EN	Prec	S.hR6			S.mP28			S.mP32			S.mP56			S.mP64			S.oF128					
			a	c	a	b	c	a	b	c	a	b	c	a	b	c	a	b	c				
US_LDA	500	H	10.240	4.021	9.328	7.454	8.930	102.7	8.018	12.759	8.654	123.9	14.436	5.808	20.243	134.6	10.530	10.286	10.268	94.8	9.958	12.262	23.550
US_LDA	247.2	H	10.198	3.961	9.245	7.384	8.842	102.9	7.934	12.656	8.527	123.7	14.301	5.747	20.033	134.6	10.384	10.210	10.146	94.3	9.818	12.144	23.386
US_LDA	197.8	M	10.087	3.762	9.142	7.344	8.413	104.1	7.680	12.548	8.184	123.1	13.954	5.607	19.630	134.8	10.143	10.038	9.813	93.3	9.489	11.867	23.141
PAW_LDA	500	H	10.232	4.009	9.320	7.470	8.881	102.8	8.004	12.743	8.637	123.9	14.422	5.800	20.229	134.7	10.521	10.259	10.259	94.9	9.936	12.247	23.523
PAW_LDA	350	H	10.210	3.992	9.287	7.424	8.863	102.8	7.962	12.704	8.584	123.9	14.355	5.773	20.147	134.7	10.455	10.236	10.201	94.6	9.886	12.209	23.433
PAW_LDA	280	M	10.147	3.872	9.155	7.350	8.710	103.3	7.826	12.570	8.375	123.6	14.153	5.672	19.842	134.7	10.255	10.132	10.008	94.0	9.685	12.016	23.229
PAW_PW91	500	H	10.971	5.526	10.479	8.182	10.481	98.5	9.586	13.896	10.894	126.8	16.666	6.634	22.955	133.5	12.183	11.882	12.118	98.7	12.202	14.626	26.100
PAW_PW91	350	H	10.887	5.191	10.539	8.138	10.231	97.7	9.288	13.680	10.502	126.4	16.297	6.513	22.484	133.6	11.798	11.563	11.753	97.9	11.669	14.158	25.688
PAW_PW91	280	M	10.735	4.411	9.928	7.849	9.506	101.8	8.553	13.251	9.374	124.6	15.378	6.152	21.356	134.1	11.104	10.900	10.935	95.8	10.641	13.006	24.809
PAW_PBE	500	H	11.042	5.432	10.678	8.265	10.578	97.7	9.469	13.913	10.835	127.1	16.599	6.603	22.830	133.4	12.007	11.738	11.980	98.3	11.951	14.267	26.115
PAW_PBE	350	H	11.068	5.358	10.564	8.304	10.483	98.3	9.502	13.822	10.684	126.6	16.490	6.573	22.701	133.4	11.961	11.766	11.984	98.1	11.911	14.524	25.846
PAW_PBE	280	M	10.823	4.603	10.047	7.896	9.673	101.4	8.799	13.313	9.553	124.8	15.636	6.237	21.690	134.1	11.282	11.072	11.122	96.0	10.823	13.081	25.184
PAW_PBE ^a	503	H	10.981	4.901	10.324	8.089	10.174	99.7	9.082	13.669	10.134	126.2	16.227	6.443	22.412	134.0	11.598	11.481	11.627	97.3	11.285	13.678	25.443
PAW_PBE ^a	402.4	M	11.063	4.638	10.189	7.827	9.891	99.7	8.971	13.498	9.752	126.1	15.788	6.304	21.768	133.2	11.369	11.196	11.224	96.5	11.083	13.519	25.079
PBEsol	500	H	10.434	4.334	9.697	7.673	9.345	101.3	8.533	13.100	9.384	124.9	15.020	6.036	21.006	134.4	11.127	10.770	10.775	95.7	10.526	12.889	24.332
PBEsol	350	H	10.450	4.292	9.6653	7.660	9.363	101.3	8.455	13.048	9.302	124.6	15.032	6.034	20.973	134.4	10.983	10.742	10.796	95.7	10.523	12.885	24.270
PBEsol	280	M	10.378	4.045	9.453	7.502	9.089	102.1	8.161	12.797	8.816	123.9	14.627	5.866	20.460	134.5	10.600	10.467	10.424	94.6	10.096	12.477	23.696
AM05	500	H	10.909	6.240	11.786	9.063	12.678	90.0	10.886	15.258	13.321	129.7	17.547	6.828	24.066	133.4	12.887	12.371	12.961	100.7	13.558	15.798	27.702
Experiment			10.9	4.27	9.68	7.641	9.409	102.1	8.442	13.025	9.356	125.0	15.096	5.998	20.951	133.9	11.102	10.96	10.9	96.7	10.465	12.866	24.486
Reference																							[54]

^a The hard sulfur pseudo-potential (S_h) is used. The standard sulfur pseudo-potential is used for all other calculations. "EN" signifies ENCIUT (the energy cut-off in eV); "Prec" signifies the setting of "precision" used. The same notations apply to Tables A.3 and A.4.

Table A.3
Calculated lattice parameters (Å) of elemental palladium and palladium sulfides compared with experimental data.

Ex. func.	EN	Prec	Pd ₄ S.tP10			Pd ₃ S.oC16			Pd ₁₆ S ₇ .cI46	PdS.tP16		PdS ₂ .oP12		
			a	a	c	a	b	c	a	a	c	a	b	c
US_LDA	500	H	3.858	5.084	5.511	6.105	5.336	7.328	8.855	6.379	6.571	5.810	5.819	5.836
PAW_LDA	500	H	3.856	5.081	5.504	6.150	5.321	7.291	8.845	6.367	6.559	5.498	5.548	6.847
PAW_PW91	500	H	3.958	5.206	5.674	6.466	5.418	7.436	9.075	6.529	6.696	5.514	5.604	8.356
PAW_PBE	500	H	3.962	5.201	5.675	6.443	5.420	7.439	9.071	6.527	6.691	5.504	5.596	8.613
PAW_PBE	350	H	3.953	5.188	5.662	6.363	5.420	7.445	9.050	6.515	6.680	5.501	5.593	8.256
PAW_PBE	280	M	3.932	5.183	5.664	6.200	5.436	7.518	9.036	6.499	6.679	5.517	5.607	7.818
PAW_PBE ^a	503	H	3.962	5.204	5.667	6.421	5.423	7.447	9.079	6.523	6.692	5.509	5.597	8.410
PAW_PBE ^a	402.4	M	3.955	5.194	5.660	6.431	5.415	7.416	9.055	6.510	6.688	5.510	6.510	6.688
PBEsol	500	H	3.892	5.122	5.563	6.189	5.371	7.363	8.920	6.420	6.604	5.475	5.548	7.390
PBEsol	350	H	3.885	5.109	5.550	6.135	5.368	7.364	8.901	6.407	6.597	5.493	5.555	7.174
PBEsol	280	M	3.868	5.113	5.537	6.004	5.388	7.407	8.888	6.381	6.612	5.529	5.591	6.862
AM05	500	H	3.888	5.112	5.558	6.169	5.370	7.356	8.910	6.421	6.599	5.441	5.530	8.119
Experiments			3.890	5.115	5.590	6.088	5.374	7.453	8.954	6.429	6.611	5.46	5.541	7.531
References			[55]		[56]			[13]	[15]		[57]			[17]

^a The hard sulfur pseudo-potential (S_h) is used. The standard sulfur pseudo-potential is used for all other calculations.

Table A.4
Calculated formation enthalpy of palladium sulfides compared with experimental data (kJ/mol).

Ex. func.	Pd ₄ S.tP10	Pd ₃ S.oC16	Pd ₁₆ S ₇ .cI46	PdS.tP16	PdS ₂ .oP12
US_LDA	-23.8	-25.4	-31	-40.2	-33.4
PAW_LDA	-24.1	-26.5	-31.7	-43.5	-34.3
PAW_PW91	-17.2	-21.1	-24.6	-35.7	-27.0
PAW_PBE	-17.4	-21.0	-24.0	-34.3	-26.3
PAW_PBE ^a	-17.6	-21.2	-24.3	-34.9	-26.7
PBEsol	-22.8	-25.4	-29.5	-40.3	-30.8
AM05	-21.4	-23.4	-26.2	-35.1	-26.0
Experiments	-19.84 ± 2.240	-24.125 ± 2.625	-25.221 ± 1.574	-39.05 ± 5.50	-26.067 ± 4.20
References	[19]	[19]	[19]	[19]	[20]

^a The hard sulfur pseudo-potential (S_h) is used with an energy cut-off of 503 eV. The standard sulfur pseudo-potential is used for all other calculations with an energy cut-off of 500 eV. All calculations are done with "high" precision.

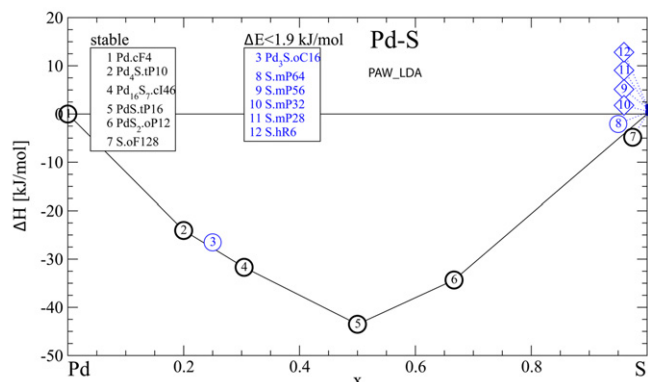


Fig. A.2. Convex hull plot of Pd-S alloys from the present DFT calculations using the PAW_LDA gradient-corrected exchange functional.

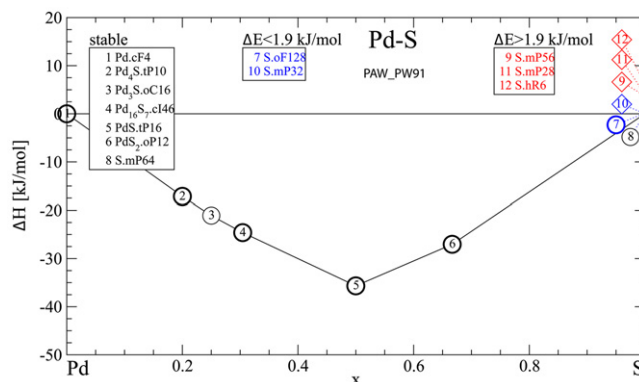


Fig. A.4. Convex hull plot of Pd-S alloys from the present DFT calculations using the PAW_PW91 gradient-corrected exchange functional.

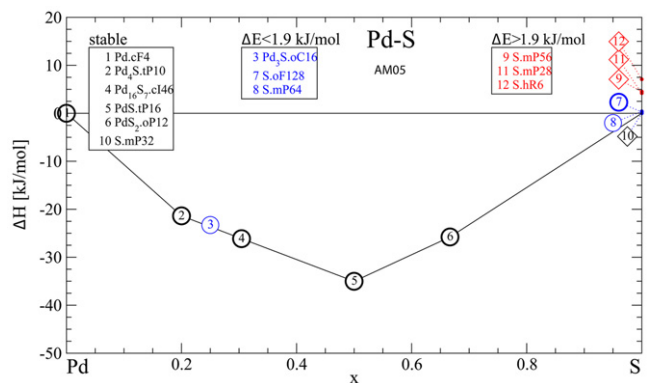


Fig. A.3. Convex hull plot of Pd-S alloys from the present DFT calculations using the AM05 gradient-corrected exchange functional.

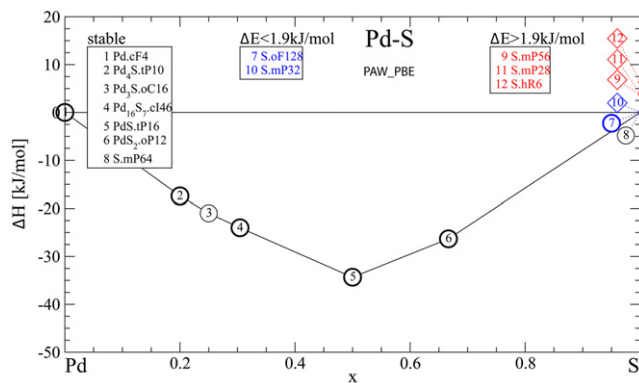


Fig. A.5. Convex hull plot of Pd-S alloys from the present DFT calculations using the PAW_PBE gradient-corrected exchange functional.

References

- [1] S. Uemiyu, Sep. Purif. Methods 28 (1999) 51–85.
- [2] S.N. Paglieri, J.D. Way, Sep. Purif. Methods 31 (2002) 1–169.
- [3] H.Y. Gao, Y.S. Lin, Y.D. Li, B.Q. Zhang, Ind. Eng. Chem. Res. 43 (2004) 6920–6930.
- [4] G.J. Stiegel, M. Ramezan, Int. J. Coal Geol. 65 (2006) 173–190.
- [5] O. Iyoha, R. Enick, R. Killmeyer, B. Morreale, J. Membr. Sci. 305 (2007) 77–92.
- [6] A. Kulprathipanja, G.O. Alptekin, J.L. Falconer, J.D. Way, J. Membr. Sci. 254 (2005) 49–62.
- [7] M.L. Burke, R.J. Madix, Surf. Sci. 237 (1990) 1–19.
- [8] F.J. Castro, G. Meyer, G. Zampieri, J. Alloys Compd. 330 (2002) 612–616.
- [9] C.H. Patterson, R.M. Lambert, Surf. Sci. 187 (1987) 339–358.
- [10] M. Kajiwara, S. Uemiyu, T. Kojima, Int. J. Hydrog. Energy 24 (1999) 839–844.
- [11] F. Weibke, J. Laar, Eur. J. Inorg. Chem. 224 (1935) 49–61.
- [12] R.J. Taylor, Metall. Trans. B 16 (1985) 143–148.
- [13] V.E. Rost, Acta Chem. Scand. 22 (1968) 819–826.
- [14] F. Gronvold, E. Rost, Acta Chem. Scand. 10 (1956) 1620–1634.
- [15] C. Romming, E. Rost, Acta Chem. Scand. 30 (1976) 425–428.
- [16] P. Matkovic, M. El-boragy, K. Schubert, J. Less-Common Met. 50 (1976) 165–176.
- [17] F. Gronvold, E. Rost, Acta Crystallogr. 10 (1957) 329–331.
- [18] H. Okamoto, J. Phase Equilib. 13 (1992) 106–107.
- [19] A. Zubkov, T. Fujino, N. Sato, K. Yamada, J. Chem. Thermodyn. 30 (1998) 571–581.
- [20] O. Kubaschewski, C.B. Alcock, P.J. Speneer, Materials Thermochemistry, Pergamon, Oxford, 1993.
- [21] K. Niwa, T. Yokokawa, T. Isoya, Bull. Chem. Soc. Jpn. 35 (1962) 1543–1545.
- [22] R.X. Hu, P. Nash, J. Mater. Sci. 40 (2005) 1067–1069.
- [23] J.P. Perdew, A. Ruzsinszky, G.I. Csonka, O.A. Vydrov, G.E. Scuseria, L.A. Constantin, X.L. Zhou, K. Burke, Phys. Rev. Lett. 100 (2008) 136406.
- [24] A.T. Dinsdale, CALPHAD 15 (1991) 317–425.
- [25] T.B. Massalski, P.R. Subramanian, H. Okamoto, L. Kacprzak, Binary Alloy Phase Diagrams, 2nd ed., vols. 1–3, ASM International, Materials Park, OH, 1990.
- [26] O. Redlich, A.T. Kister, Ind. Eng. Chem. 40 (1948) 345–348.
- [27] I. Ansara, B. Sundman, in: P.S. Glaeser (Ed.), Computer Handling and Dissemination of Data, 1987.
- [28] B. Sundman, B. Jansson, J.O. Andersson, CALPHAD 9 (1985) 153–190.
- [29] G. Kresse, J. Hafner, Phys. Rev. B 47 (1993) 558–561.
- [30] G. Kresse, J. Furthmueller, Phys. Rev. B 54 (1996) 11169–11186.
- [31] D. Vanderbilt, Phys. Rev. B 41 (1990) 7892.
- [32] P.E. Blochl, Phys. Rev. B 50 (1994) 17953.
- [33] H.J. Monkhorst, Phys. Rev. B 13 (1976) 5188.
- [34] M. Methfessel, A.T. Paxton, Phys. Rev. B 40 (1989) 3616.
- [35] P. Villars, L.D. Calvert, Pearson's Handbook of Crystallographic Data for Intermetallic Phases, ASM International, Materials Park, OH, 1991.
- [36] P.C. Aeberhard, J.S. Arey, I.C. Lin, U. Rothlisberger, J. Chem. Theory Comput. 5 (2009) 23–28.
- [37] B. Hammer, L.B. Hansen, J.K. Norskov, Phys. Rev. B 59 (1999) 7413–7421.
- [38] J.P. Perdew, A. Zunger, Phys. Rev. B 23 (1981) 5048–5079.
- [39] J.P. Perdew, J.A. Chevary, S.H. Vosko, K.A. Jackson, M.R. Pederson, D.J. Singh, C. Fiolhais, Phys. Rev. B 46 (1992) 6671–6687.
- [40] J.P. Perdew, K. Burke, M. Ernzerhof, Phys. Rev. Lett. 77 (1996) 3865–3868.
- [41] R. Armiento, A.E. Mattsson, Phys. Rev. B 72 (2005) 085108.
- [42] A.E. Mattsson, R. Armiento, J. Paier, G. Kresse, J.M. Wills, T.R. Mattsson, J. Chem. Phys. 128 (2008) 084714.
- [43] A.E. Mattsson, R. Armiento, Phys. Rev. B 79 (2009) 155101.
- [44] C. Wolverton, X.Y. Yan, R. Vijayaraghavan, V. Ozolins, Acta Mater. 50 (2002) 2187–2197.
- [45] Y. Wang, S. Curtarolo, C. Jiang, R. Arroyave, T. Wang, G. Ceder, L.Q. Chen, Z.K. Liu, CALPHAD 28 (2004) 79–90.
- [46] G. Ghosh, M. Asta, Acta Mater. 53 (2005) 3225–3252.
- [47] S. Curtarolo, D. Morgan, G. Ceder, CALPHAD 29 (2005) 163–211.
- [48] M.H.F. Sluiter, CALPHAD 30 (2006) 357–366.
- [49] M.C. Gao, A.D. Rollett, M. Widom, Phys. Rev. B 75 (2007) 174120.
- [50] J.D.H. Donnay, Acta Crystallogr. 8 (1955) 245–246.
- [51] R. Steudel, J. Steidel, J. Pickardt, F. Schuster, R. Reinhardt, Z. Naturforsch. B: Anorg. Chem., Org. Chem. 35 (1980) 1378–1383.
- [52] Y. Watanabe, Acta Crystallogr. B 30 (1974) 1396–1401.
- [53] D.E. Sands, J. Am. Chem. Soc. 87 (1965) 1395–1396.
- [54] S.J. Rettig, J. Trotter, Acta Crystallogr. C 43 (1987) 2260–2262.
- [55] I.R. Harris, M. Norman, W.E. Gardner, J. Less-Common Met. 29 (1972) 299–309.
- [56] F. Gronvold, E. Rost, Acta Crystallogr. 15 (1962) 11–13.
- [57] N.E. Brese, P.J. Squattrito, J.A. Ibers, Acta Crystallogr. C 41 (1985) 1829–1830.